Simulation of solid specimen for compression tests by discrete particles

A. Maknickas*, R. Kačianauskas**, R. Kutas***

*Vilnius Gediminas Technical University, Saulėtekio 11, 10223 Vilnius, Lithuania, E-mail: alm@sc.vgtu.lt
**Vilnius Gediminas Technical University, Saulėtekio 11, 10223 Vilnius, Lithuania, E-mail: rkac@fm.vgtu.lt
***Vilnius Gediminas Technical University, Saulėtekio 11, 10223 Vilnius, Lithuania, E-mail: rk@sc.vgtu.lt

1. Introduction

Among various numerical techniques, the discrete (distinct) element method (DEM) became widely recognised after the pioneering work published by Cundall [1] and later work of Cundall and Strack [2]. The representation of granular media as an assembly of contacting particles termed hereafter as discrete elements was seen as a more realistic approach compared to continuum models. In the DEM, the particles of granular media are treated as individual objects and all dynamical state variables of each particle are tracked during the simulation. The DEM allows the simulation of motion and interaction between the particles, taking into account the microscopic geometry and various constitutive models.

The main advantage of DEM is a possibility to model highly complex poly-dispersed systems using the basic data on individual particles without making oversimplifying assumptions. This makes DEM different from the conventional discretization methods used in the continuum mechanics, such as the finite difference, finite element and boundary element methods, helping to avoid difficulties encountered in describing the microscopic nature of the granular media at the continuum level.

Basically, the DEM as computational methodology of DEM responds to physical nature of granular materials. Among huge amount of comprehensive research some review papers may be recommended (Herrmann and Luding [3], Džiugys and Peters [4], Tomas [5], Kruggel-Emden et. al. [6]). The DEM is a multidisciplinary subject comprising fundamental concepts of molecular dynamics, Allen et. al. [7], Pöschel and Schwager [8] and traditional Finite Element Method, Munjiza [9]. Concerning computational procedure, the most detailed and transparent presentation of algorithmic structure and the details of the DEM are given by Peters and Džiugys [10]. Different programming approaches used for the development of sequential software codes for discrete element method and performance of separate procedures are investigated in [11]. In addition to various granular problems comprising particle motion in hopper [12], compacting (Procopio and Zavaliangos [13], axissymmetrical particle flow Markauskas [14]), segregation (Džiugys et. al. [15]), the application of DEM to solid problem also plays a significant role.

Various aspects and problems are faced in simulation of solid bodies by applying DEM technique. It is widely recognised that the macroscopic properties of the particulate assemblies depend on their single particle properties and the interaction between contiguous particles, while modelling of the mechanical behaviour of particulates can be reflected by inter-particle stiffness models. The influence of stiffness on the microscopic and macroscopic deformation characteristics of differently shaped particulate assemblies is considered by Moreno-Atanasio and Antony [16].

The fundamental issues such, as selection of realistic inter – particle modulus, evaluation of relationships between microscopic characteristics of particles and macroscopic characteristics of the solid body are related to the generation of particle composition. Various models have been investigated in the works of Hentz et. al. [17], Antonyuk et al. [18], Mishra and Thornton [19], D'Addetta and Ramm [20].

Simulation of solid body by particles requires generation of the initial state of particles, which may be regarded as generation of the initial conditions. In any case, artificial simulation stage will be required [17, 20, 21] for these purposes. This may be done by slightly different approaches. It is observed that this initial simulation stage may affect the final result, however, a unified approach is still under development.

The paper presents a physically adjustable concept for the simulation of solid specimen for compression test. This type of tests is widely used for the evaluation of material properties. A particular emphasis is placed on the integrity of generation scenario containing contact-free and contacting phases in compacting and load-free stabilization phase. The approved scenario is illustrated by applying mono-sized and poly-disperse assemblies of particles.

2. Discrete concept and methodology

The time-driven (TD) discrete element method as originally proposed in [1], is explored to simulate the behaviour of granular material. This method is better suited for a longer time of particle collision than for free path of particles.

Granular material is regarded as a system of the finite number N of spherical particles, characterised by radii R_i ($i = 1, \ldots, N$) and the prescribed material properties.

The dynamical behaviour of an individual particle i is considered by applying the Newton's second law. Three independent translations and three independent rotations expressed in terms of the forces and torques at the centre of the particle are as follows

$$m_i \frac{d^2 \boldsymbol{x}_i}{dt^2} = \boldsymbol{F}_i \tag{1}$$

$$I_i \frac{d^2 \boldsymbol{\theta}_i}{dt^2} = \boldsymbol{T}_i \tag{2}$$

here m_i, and I_i are mass and inertia moments, while vectors $\boldsymbol{x}_i$ and $\boldsymbol{\theta}_i$ initiate the position of the particle centre and the

orientation of particle i, respectively. Vectors $\boldsymbol{F}_i$ and $\boldsymbol{T}_i$ present the sum of external contact force, and gravity force as well as the corresponding torques.

The main focus of the TD methods is on evaluation of contact forces

$$\boldsymbol{F}_i = \sum_{j=1, j\neq i}^{N} \boldsymbol{F}_{ij} + m_i \boldsymbol{g} \tag{3}$$

$$\boldsymbol{T}_i = \sum_{j=1, j\neq i}^{N} \boldsymbol{T}_{ij} = \sum_{j=1, j\neq i}^{N} \boldsymbol{d}_{cij} \times \boldsymbol{F}_{ij} \tag{4}$$

where $\boldsymbol{d}_{cij}$ is particle geometry-dependent vector, pointing from the particle centre to contact centre.

The particle deformation due to collision is assumed to be approximated by the overlap area of the spheres. The contact point C_{ij} is defined to be in the centre of the overlap area with the position vector $\boldsymbol{X}_{cij}$. The depth of overlap h_{ij} is defined by expression

$$h_{ij} = \alpha\left(R_i + R_j\right) - \left|\boldsymbol{x}_{ij}\right| \tag{5}$$

and is provided that it is much smaller than the particles radii Ri and Rj, where interaction area of particles is

$$h_{ij} > 0 \tag{6}$$

here, $\alpha \geq 1$ is overlap factor used for artificial connection of the particles in neighbourhood. In most carry of granular material $\alpha = 1$.

Methodology of calculating the forces Eqs. (3)-(4) depends on the particle geometry and mechanical properties as well as on the constitutive model of the particle interaction. The presented inter-particle contact model considers a combination of elasticity, viscous damping and friction force effects. Actually, the contact between two material particles is modelled by a unilateral spring and dashpot in the normal and spring and dashpot as well an additional slider in tangential direction.

Hence, the inter-particle contact force vector $\boldsymbol{F}_{ij}$ describing the contact between the particles i and j may be expressed in terms of normal and the tangential components $\boldsymbol{F}_{ij}^n$ and $\boldsymbol{F}_{ij}^t$, respectively. The normal direction of the contact surface is defined by a unit vector $\boldsymbol{n}_{ij}$ extending through the centre of the overlap area. The unit vector $\boldsymbol{t}_{ij}$ of the tangential contact direction is perpendicular to $\boldsymbol{n}_{ij}$.

The normal component $\boldsymbol{F}_{ij}^n$ presenting, actually, a repulsion force comprises elastic and viscous ingredients. The tangential component $\boldsymbol{F}_{ij}^t$ reflects static or dynamic frictional behaviour. The static force describes friction prior to gross sliding and comprises elastic and viscous ingredients, while the dynamic force describes friction after gross sliding and is expressed by the Coulomb's law. Contact behaviour is characterized by microscopic parameters such as interaction stiffness k_{ij}^n, k_{ij}^t and damping coefficients γ_n and γ_t, which may be explicitly expressed in terms of interacting particle data. Inter-particle friction is defined by internal friction coefficient μ which may be different, depending on whether particle-particle or particle-wall contact is considered.

When overlap parameters Eqs. (5)-(6) are known, contact forces acting between two particles may be evaluated explicitly. For Hook contact model, the forces are

$$\boldsymbol{F}_{ij}^n = k_{ij}^n h_{ij} \boldsymbol{n}_{ij} - \gamma_n m_{ij} \boldsymbol{v}_{ij}^n \tag{7}$$

$$\boldsymbol{F}_{ij}^t = -\boldsymbol{t}_{ij}\, min\left(\left|-k_{ij}^t \sqrt{h_{ij}}\,\boldsymbol{\delta}_{ij}^t - \gamma_t m_{ij} \boldsymbol{v}_{ij}^t\right|, \mu\left|\boldsymbol{F}_{ij}^n\right|\right) \tag{8}$$

where m_{ij} is reduced mass, $\boldsymbol{v}_{ij}^n$ is normal velocity of contact centre, $\boldsymbol{\delta}_{ij}^t$ is tangential displacement vector, $\boldsymbol{v}_{ij}^t$ is tangential velocity of contact centre. The stiffness parameters are defined as

$$k_{ij}^n = \frac{2}{3}\cdot\frac{E}{\left(1-\nu^2\right)}R_{ij} \tag{9}$$

$$k_{ij}^t = \frac{8}{3}\cdot\frac{G\sqrt{R_{ij}}}{\left(2-\nu\right)} \tag{10}$$

where E is elastic modulus, G is shear modulus, ν is Poisson coefficient and R_{ij} reduced radius of particles.

For evaluating the contact force vector $\boldsymbol{F}_{ij}$ in (3), all contacts between the particles and their neighbours must be detected. Generally, contact detection problem is of the size $O(N^2)$ for the system containing N particles. In order to reduce the number of all particle pair combinations, a simple cellular decomposition known as *link-cell* method [22] was used for contact detection. A detailed description of the DEM technique applied may also be found in [23, 24].

The dynamical state of granular material is determined by numerical integration of Eqs. (1)-(2). In order to find a reasonable compromise between accuracy and computational efficiency, explicit one-step or predictor–corrector integration schemes are mainly used [25].

The predictor-corrector scheme represents a two-step procedure. Let us denote the time dependent variables, positions $\boldsymbol{x}_i$, velocities $\boldsymbol{v}_i = d\boldsymbol{x}_i/dt$, accelerations $\boldsymbol{a}_i = d^2\boldsymbol{x}_i/dt^2$ and the higher-order time derivatives $\boldsymbol{b}_{3i} = d^3\boldsymbol{x}_i/dt^3$, $\boldsymbol{b}_{4i} = d^4\boldsymbol{x}_i/dt^4$ and $\boldsymbol{b}_{5i} = d^5\boldsymbol{x}_i/dt^5$ of particle i by vector $y_i = \left\{x_i, v_i, a_i, b_{3i}, b_{4i}, b_{5i}\right\}^T$. The new value variables at time increment $t+\Delta t$ are predicted by a simple series expansion up to a desired order of accuracy

$$\boldsymbol{y}_i^p\left(t + \Delta t\right) = \boldsymbol{y}_i\left(t\right) + \Delta\boldsymbol{y}_i^p\left(\Delta t\right) \tag{11}$$

Here, incremental vector $\Delta\boldsymbol{y}_i^p\left(\Delta t\right)$ presents the required terms of the expansion series. Then, according to the new positions and velocities, the particle forces and accelerations are corrected and acceleration increment $\Delta\boldsymbol{a}_i$ is updated. Finally, the vector of particle variables is corrected as follows

$$\boldsymbol{y}_i^c\left(t + \Delta t\right) = \boldsymbol{y}_i^p\left(t + \Delta t\right) + \Delta\boldsymbol{y}_i^c\left(c_j, \Delta t, \Delta\boldsymbol{a}_i\right) \tag{12}$$

Here, the correction vector $\Delta\boldsymbol{y}_i^p$ is calculated by using the given integration constants c_j. For details the [10] may be referred.

The discussed methodology was implemented

into the original DEMMAT code [24], which was employed for described simulation below.

3. Problem formulation and basic data

For the simulation of solid specimen for compression tests the following scenario is proposed. It comprises several implementation steps: contact free multiaxial compaction, multiaxial compaction of contacting particles, load-free simulation after instant fragmentation and, finally, axial compression.

The three-dimensional computational domain containing particles presents a box in the form of a rectangular parallelepiped (Fig. 1). The dimensions of the box sides are equal to those usually used for standard concrete specimens, assuming that the ratio of longitudinal specimens height, H, and cross sectional dimension, a, are equal to 4 (hence, $H = 160$ mm, $a = 40$ mm).
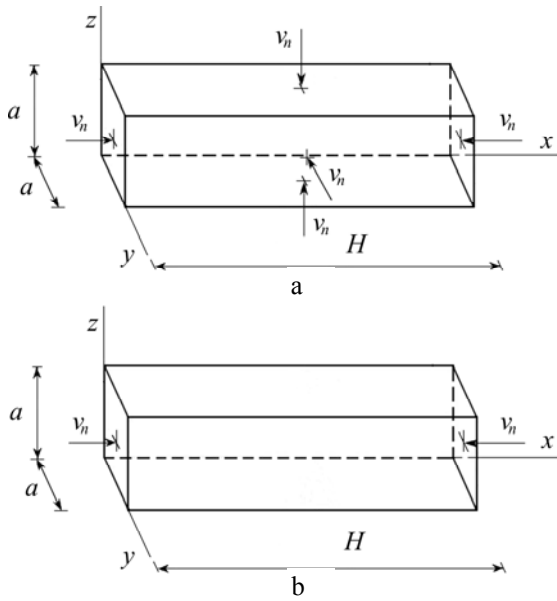

Fig. 1 Illustration of the material loading: a - multiaxial compression, b - uniaxial compression

Basic physical parameters of the particles used throughout simulation are presented in Table 1.

It should be noted that the microscopic data of particles ρ, E and v are assumed to be the same as the macroscopic values obtained during the experiment of specimen made of cement used for refractory concrete.

Table 1

Physical data of particles

Quantity	Value
Particle density ρ	2300 kg/m^3
Normal Young's modulus E	13 GPa
Poisson's ratio v	0.2
Normal damping coefficient γ_n	150 s^{-1}
Shear damping coefficient γ_t	100 s^{-1}
Particle-particle friction coefficient μ	0.3
Particle-wall friction coefficient μ_w	0.0

Here, the values of the viscous damping coefficient γ are prescribed on the basis of values given in references and rely on personal computational experience. Frictional properties are defined by particle-particle friction coefficients μ exhibit a relatively rough material with perfect sliding on the wall.

Two compositions were generated for the purpose of simulation. The monosized material was simulated by 3500 particles with the diameter $d = 1.9$ mm. The initial composition of the particles presents a homogeneous orthogonal lattice type structure, where particles are embedded into the centres of cells to ensure that they are not in contact at the beginning of motion.

The lattice structure is defined by 40x10x10 cells with the maximum number of cells, usual equal to 4000. After creating of material part of the cells remain empty, so giving the form for compaction. The chart of the initial composition is given in Fig. 2.
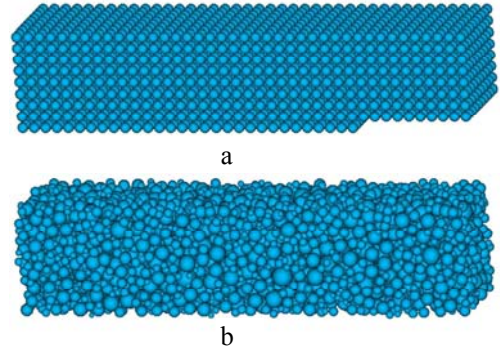

Fig. 2 The initial composition of particles: a - monosized material; b - polydispersed material

In the framework of the current investigation, generation of the polydispersed material is performed by a constructive algorithm as proposed in [26]. Polydispersive character of the composition of particles of different sizes is characterized by the heterogeneity ratio between the maximal and minimal diameters of the particles

$$\alpha = \frac{d_{max}}{d_{min}} \tag{13}$$

and the normal distribution law. Finally, the material is defined by the up-scaled size distribution curve and given characteristic particle diameter. The polydispersed materials with $\alpha = 4.3$ will be used in the simulations described below.

For generating the required particle composition and locating particles in the given initial space the algorithm presented by Jiang et.al. [27] was utilized. The algorithm runs iteratively and, after some trial and error cycles, a relatively dense contact less particle composition is obtained. The number of particles or the particle volume may be controlled within the prescribed limits. By applying the above algorithm, 3499 particles with maximal diameter, $d_{max} = 3.925$ mm and $d_{min} = 0.918$ mm, were generated. The obtained composition (Fig. 2, b) was applied in further simulation.

4. Simulation of compression and the results obtained

Motion of the particles is obtained by numerical integration of Eqs. (1)-(2). For the explicit integration schemes [5, 6], it is obtained in terms of the particle mass m and stiffness k_v

$$\Delta t = \frac{\pi}{2\beta}\sqrt{\frac{m}{k^n}} \qquad (14)$$

here, k^n is defined according to Eq. (9). The factor $\beta = 20$ is assumed in our examples. The values of the time integration step Δt were predefined by the size of the smallest particle. Finally, the time step equal to $\Delta t_m = 0.295$ μs for monosized specimen and $\Delta t_p = 0.143$ μs for polydispersed material was applied.

4.1. Multiaxial compaction

In order to form the specimen, the initially generated domain filled with contact less particles was subjected to triaxial compression (Fig. 1, a). The compaction was performed by the motion of rigid walls and controlled in time t by a constant rate v_n, ($v_n = 0.01$ m/s). In order to reach the solid state, the compaction time $T_p = 0.237$ s was required for polydispersed material and $T_m = 0.432$ s – for monosized material. The size of the polydisperse specimen was reduced under compression by 11.85 and 2.96%, respectively, in the transverse and longitudinal directions, while monosized specimen was reduced by 21.6 and 5.4%, respectively.
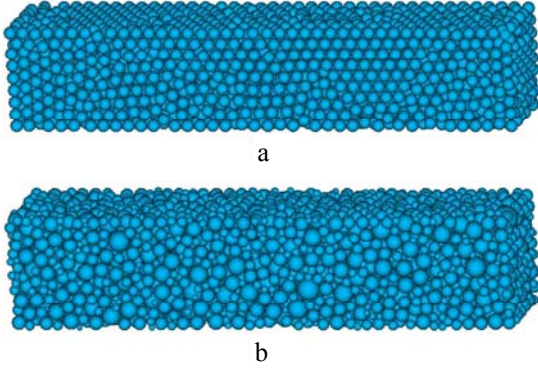

Fig. 3 Final state of the compacted material of contact-free particles: a - mono-sized, b - poly-dispersed

Final states of the compacted material are presented in Fig. 3. They exhibit particle behaviour of different nature. The rectangular cells have a tendency to be transformed into pyramidal (triangle) lattice. This tendency is not fully accomplished because of the lack of the free space and the influence of boundaries. The triangle structure prevails in the middle part, while the rectangular structure remains near the ends. The completely chaotic rearrangement is observed in the polydispersed specimen.

Compaction comprises two different phases of the material behaviour. The initial contactless phase may be considered as a gas phase. Let us consider time variation of internal variables. The transformation to the solid phase was controlled by considering time variation of the side wall pressure $p(t)$ and packing density $D(t)$ (Fig. 4). In the gas phase, the wall pressure variation remains zero (Fig. 4, a), while transformation to a solid phase is indicated by the jump. Transition time $T_{1M} = 0.349$ s for monosized and $T_{1P} = 0.137$ s for polydispersed material is clearly indicated in the figure.

Thus, the obtained time required to reach the solid phase for polydisperse material is considerably shorter than this time for monosized material. This difference shows

that the initial conditions, however, were more favourable for compacting the polydispersed particles than the monosized ones.
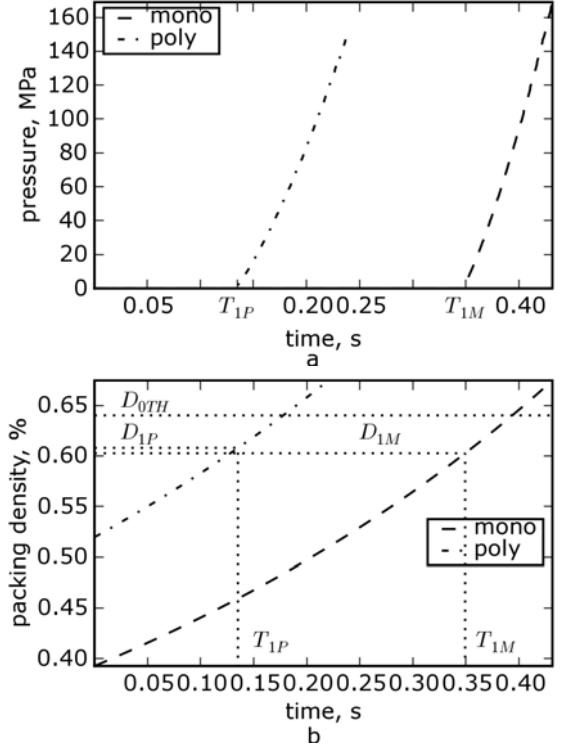

Fig. 4 Time variations of the wall pressure (a) and packing density (b)

Quality of the contact-less compaction is illustrated by the values of transitional packing densities. The transitional density $D_{1M} \approx 0.60$ for the monosized material approaches the theoretical limit $D_{0TH} \approx 0.64$ [28], which illustrates the acceptable quality of the simulations. The polydispersed material, with $D_{1P} \approx 0.61$, exhibits slightly better simulation quality.

Compaction of a solid phase may be also examined by considering wall pressures and coordination numbers as the functions of the packing density

Variation of the coordination number versus the packing density is plotted in Fig. 5 The graphs shown clearly illustrate the microscopic behaviour of granular materials and phase change during compaction.

It should be noted that higher values of packing densities, as depicted in Fig. 4, b and Fig. 5 are addressed for the formation of crystaline-like structures and the exertion of the particles deformations.

The second phase is characterized as the bulk solid phase, where particles come into contact with each other, while densification is possible due to the particles' rearrangement and microscopic deformation of the contacting particles. The solid phase is characterized, finally, by a stable structure of particles, forming a contact force network.

Generally, the coordination number varies between two limits. The lower limit Z_{min} denotes the initiation of the solid phase. For the monosized material $Z_{1min} = 5.72$, while for the polydispersed material $Z_{2min} = 4.292$. The upper limit characterises the imaginary ideal packing structure. In the case of monosized material, perfect structure would be tetrahedral with $Z_{max} = 8$, thus numerically ob-

tained value $Z_{max} = 6.9$, reflects the deficiency of the lattice structure. For polydispersed material a definition of the ideal structure would require some specific investigation.
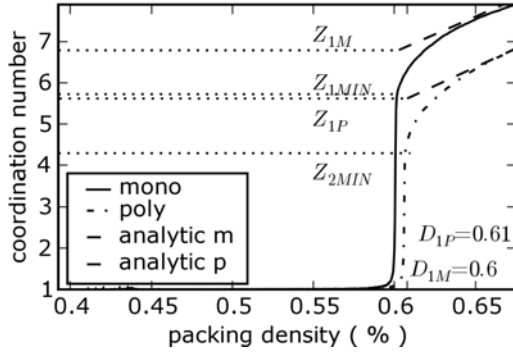

Fig. 5 Variation of coordination number versus packing density

Analytical description of the relationship between coordination number Z and density D is given by Arzt [29] and Fleck [30]. For monosized packing, the increase in average coordination number against relative density has been modelled by analytical approaches that consider either the concentric growth of a particle in a Voronoi cell [29] or the reduction of the centre to centre spacing between two representative particles [30]. For the isostatic conditions it reads:

$$Z = Z_0 + C\left(\left(\frac{D}{D_i}\right)^{\frac{1}{3}} - 1\right)$$ (15)

here, D_i and D are the initial and current relative densities of the powder compact, while Z_0 is initial coordination number and C is constant.

For describing the numerical results according to best fit asymptotic constant values $Z_0 = Z_{1M} = 6.8$, $C = 30$ and $D_i = D_{1M} = 0.60$ were used for monosized material, while $Z_0 = Z_{1P} = 5.6$, $C = 35$ and $D_i = D_{1P} = 0.61$ were used for polydispersed material.

The analytically according to Eq. (10) obtained curves are added to the graph in Fig. 5. The picture illustrates good agreement with the numerical results.

In order to examine the quality of the solid compaction, the relationship between wall pressure p and density D was also studied. Analytical description of the above relationship $p = P(D)$ was derived based on the experimental results of Sridhar and Fleck [31]. The power law with the power factor 5/4 was established and the following formula was suggested for analytical description

$$p = p_c\left(D - D_c\right)^{\frac{5}{4}}$$ (16)

It is valid when, $D > D_c$, while p_c and D_c are constants.

The relevance of analytical approximation was checked by using least square approximation by introducing the dimension quality factor f varying between 0 and 1 as follows

$$f = \frac{1}{1 + \delta}$$ (17)

$$\delta^2 = \frac{\sum_i \left(\frac{(p - p_{ai})}{p_{ai}}\right)^2}{n}$$ (18)

The perfect confidence would yield $f = 1$, where, p stands for experimental curve, while p_{ai} denotes the results of approximation. The values of experimental fitness with analytical function are given in Table 2.
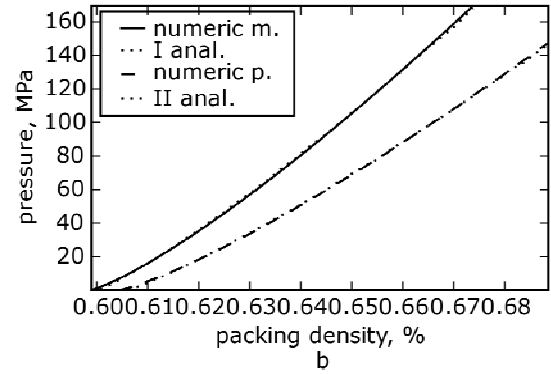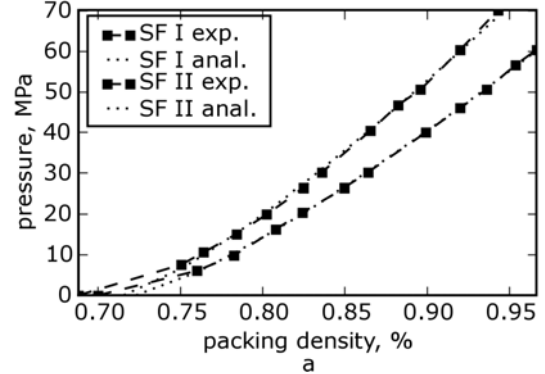

Fig. 6 Pressure curves: a - analytical approach and experiment (Sridhar et al.); b - analytical approach and theoretical calculation

The relevance of the suggested expression was proved against two experimental curves given in [31]. Basing on that, the constants p_c and D_c were obtained. The values of p_c constants were taken from the graph in Fig. 6.

Table 2

Constants of the pressure curves

Material	D_c	p_c	f
SF I	0.71552	436.6441	0.847513
SF II	0.722977	351.7507	0.889686
DEM poly	0.604162	3237.276	0.797388
DEM mono	0.598595	4299.227	0.822893

The values of the constants are given in Table 1, while graphical illustration of the experimental curves SF I exp and SF II exp, as well analytical by obtained results SF I anal and SF II anal are presented in Fig. 6, a. It is obvious that analytical approximation is practically valid for the entire range except for the first point.

The suggested expression (15) was better applied to evaluating of the DEM simulation results. A comparison of the results is also presented in Table 2 and illustrated in Fig. 6, b. Based of these results it could be stated that DEM simulation describes the nature of compaction and the

compacted state be regarded as a physically adjustable.

4.2. Fragmentation and stabilization of the specimen

The main aim of the present simulations was to generate a specimen as a solid body composed, however, of particles. Actually, this body consists of real granules and binding matrix, while microscopic interparticle forces are neglected at the macroscopic level.

Assuming that the compacted particles present a desired body, instant fragmentation would be the simplest artificial procedure to achieve the final goal. Two main differences between the physical state of the simulated granular packing and the real solid body should be outlined.

Firstly, it concerns the internal forces. In the ideal case, granular packing should have the maximal density with almost zero selfequilibrium interparticle forces. In our case, densification is achieved due to of increased particles' overlap, resulting in the increase of interparticle forces. Secondly, the real binding matrix of material is simply considered as an empty space. This simplification directly affects interparticle contacts and is characterized in terms of the reduced values of the coordination number.

Transformation of granular packing to the solid body was implemented by instant fragmentation. Fragmentation occurs when side walls are removed. The unilateral interparticle model was replaced by bilateral interparticle springs. The interparticle forces are obtained accordingly to conventional expressions (7), however, physical meaning is slightly different. Original expression (7) is applied for calculation of repulsion force. In the case of attractive (tension) force overlap h_{ij} obtained according to Eq. (5) is replaced by interparticle displacement

$$h_{ij} = \left| x_{ij} \right| - R_i - R_j \qquad (19)$$

valid upon condition

$$R_i + R_j \le \left| x_{ij} \right| \qquad (20)$$

The influence of the binding matrix was incorporated by increasing the coordination number. It was done by increasing the particles overlap in Eq. (5) characterized by the factor α ranging from 1.1 to 1.6.

Fragmentation of the specimen was performed by introducing overlap factor $\alpha = 1.4$ for the monosized and for the polydispersed sample. Consequently, it yielded a jump of the coordination number Z from 8 up to 10.49 and from 6.9 up to 10.3 for monosized and polydispersed materials, respectively.

The stabilisation phase continued for 0.06 s. It may be characterised by permanent expansion of the specimen. The behaviour of the particles is illustrated by considering translational and rotational energy of the particles (Fig. 7). It is clearly observed that a considerable reduction of energy occurred practically instantaneously, in a short time interval of 0.15 s. The fluctuations of energy are practically stable at the end of the time period under consideration. However, the curves exhibit different energy levels, which are by two orders lower for the polydispersed example.

There is no direct possibility to diminish the in-

ternal forces. It is clear that this influence became smaller with the increase of the number of particles or heterogeneity ratio. The influence of the internal forces in the artificially generated body may be evaluated indirectly by examining distortion in the shape, while the distortion magnitude may be considered as quality indicator.
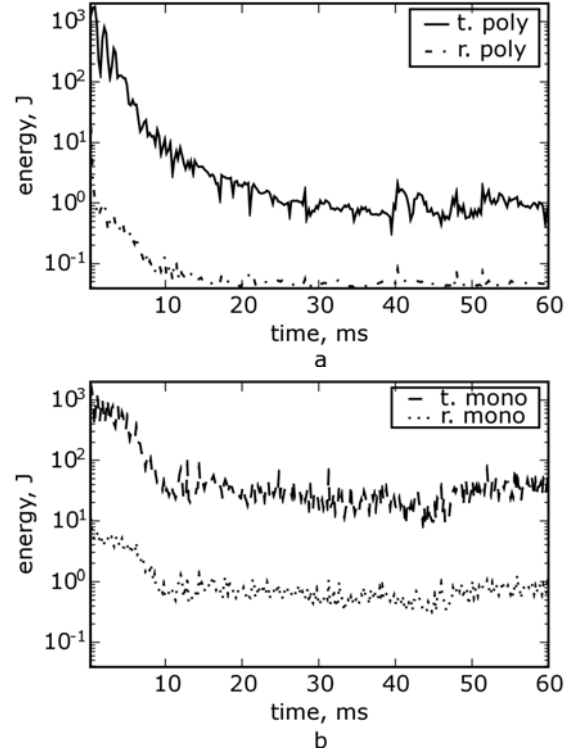

Fig. 7 Translational and rotational kinetic energy: a - polydispersed; b - monosized specimen
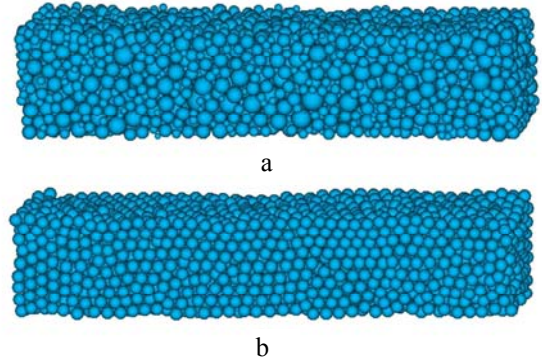

Fig. 8 Final state of the generated specimen: a - polydispersed; b - monosized

The final states of two generated specimens are presented in Fig. 8. Quantitatively, the final shape is characterized by the largest 0.11% distortion for monosized and by 0.07% distortion for the polydispersed material models.

Qualitatively, the largest distortions occur at the specimen ends. Explanation follows that particles located in the end regions have got smaller space for rearrangement during compacting. In may by concluded, the obtained shapes exhibit good quality for the simulation of compression.

A different character of the deformation behaviour of both specimens is illustrated by considering the motion of particles during deformation. The trajectories of

100 randomly selected particles were shown for the sake of illustration. The particles of the monosized specimen exhibit strong transversal motion that causes a large deformation of cross section during deformation. The motion of polydispersed specimen (Fig. 9, b) exhibits the chaotic character of trajectories. This local self-equilibrium mechanism leads to lower global deformation.
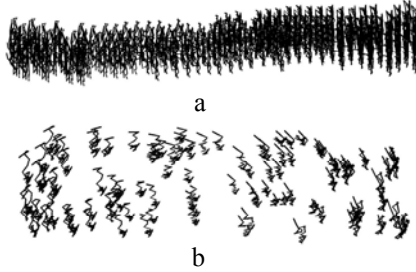

Fig. 9 Trajectories of the hundred randomly selected particles: a - monosized solid material; b - polydispersed solid material

4.3 Uniaxial compression

Uniaxial compression is a testing procedure employed for the evaluation of physical parameters and macroscopic behaviour of solid materials For realistic simulation of the macroscopic behaviour, the proper relationship between microscopic and macroscopic parameters is required. However, the detailed examination of these relationships will be beyond the scope of current paper. Our focus is on the the most important quantity, elasticity modulus E.

The relaxed state of the particles is used further in numerical simulation. Uniaxial compression is implemented (Fig. 1, b) by the motion of two rigid end-walls with velocity $v_n = 0.1$ m/s. Compression starts when the stabilisation is assumed to be achieved.

Compression results are presented in Fig. 10. Graph results show the relationship between wall pressure and axial strain. The tangents of the curves indicate the character of the elasticity modulus.
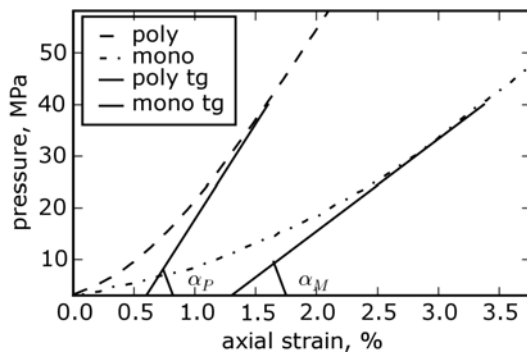

Fig. 10 Pressure-strain relationship during compression for various materials

It could be observed that initial deformation stage reflects influence of microscopic changes vanishing by increase of loading. The macroscopic elasticity modulus as a tangent of deformation curve could be extracted from the linear segment.

Thus, polydispersed material yields elasticity modulus $E_P = 3.7$ GPa, while monodispersed material yields elasticity modulus $E_m = 1.78$ GPa. The above values are below the applied microscopic value $E_{micr} = 13.0$ GPa. The results obtained illustrate that two different compositions of particles with identical micromechanical properties finally yield different macroscopic elasticity modules.

Therefore, polydispersed composition preventing the formation of the crystalline-like structure, yields smaller difference between microscopic and macroscopic parameters and is preferable for simulations of uniaxial compression. The obtained values fit expectation, however, detailed calibration of the parameters acquires futures investigations.

5. Conclusions

Simulation of solid specimen for the compression test was examined. The suggested scheme comprises tri-axial compacting and load-free stabilization after fragmentation. Compaction of contact less particulate material responds to the phase of granular gas, while transition to bulk solid is controlled by packing density values of wall pressures and jump coordination number. On the basis of the numerical results obtained for monosized and poly-dispersed materials the following conclusions have been drawn.

1. The quality of contact less compaction was checked by the obtained values of packing density. The results for monosized material, yielding 6.25% difference compared to theoretical limit ($D_{th} = 0.64$), reflected the quality with sufficient accuracy.

2. For evaluating the wall pressure a new analytical formula was suggested. The expression was validated by the already known experimental results and the agreement was observed.

3. Final compaction of contacting particles was controlled by the limit value of packing density D and evolution of coordination number Z and wall pressure p. It was found that for monosized material the coordination number Z practically reached the limit, while time variation of Z and p fitted analytical predictions.

4. The final shape after relaxation is characterized by smaller distortions and a lower kinetic energy level for polydispersed material models.

5. Results fit general tendency that in reliable simulation of solid body by particles microscopic elastic modulus is considerable higher compared to macroscopic. Precise relationship between both parameters is predefined by contact force network, while polydisperse model is preferable against monosized composition.

6. The suggested simulation scenario is physically observable; therefore it has some advantages over more simple but more artificial simulations. It allows us to control the inside of the ongoing processes in practically observable limits. However, more comprehensive research is still required for evaluating particles' composition.

References

1. **Cundall, P.A.** A computer model for simulating progressive large scale movements in blocky rock systems. -Proc. of the Symposium of the International Society of Rock Mechanics. -Nancy, France, 1971, 1; Paper No.II-8.

2. **Cundall, P.A., Strack, O.D.L.** A discrete numerical

model for granular assemblies. -Geotechnique, 1979; 29(1), p.47-65.

3. **Herrmann, H.J., Luding, S.** Modelling granular media on the computer. -Continuum Mech. Thermodyn., 1998, 10, p.189-231.

4. **Džiugys, A., Peters, B.J.** An approach to simulate the motion of spherical and non-spherical fuel particles in combustion chambers. -Granular Material, 2001, 3(4), p.231-266.

5. **Tomas, J.** Fundamentals of cohesive powder consolidation and flow. -Granular Matter, 2004, 6, p.75-86.

6. **Kruggel-Emden, H., Simsek, E., Rickelt, S., Wirtz, S. and Scherer, V.** Review and extension of normal force models for the Discrete Element Method. -Powder Technology, 2007, 171(26), p.157-173.

7. **Allen, M.P., Frenkel, D., Talbot, J.** Molecular dynamics simulation using hard particles. -Computer Physics Reports, 1989, 9, p.301-353.

8. **Pöschel, T., Schwager, T.** Computational Granular Dynamics. -Models and Algorithms. –Berlin: Springer, 2004.-322p.

9. **Munjiza, A.** The Combined Finite-Discrete Element Method. –London: Wiley, 2004.-333p.

10. **Peters, B.J., Džiugys, A.** Numerical simulation of the motion of granular material using object-oriented techniques. -Comput. Methods Appl. Engrg., 2002, 191, p.1983-2007.

11. **Balevičius, R., Džiugys, A., Kačianauskas, R., Maknickas, A., Vislavičius, K.** Investigation of performance of programming approaches and languages used for numerical simulation of granular material by the discrete element method. -Computer Physics Communications, 2006, 175, p.404-415.

12. **Balevičius, R., Markauskas, D.** Numerical stress analysis of granular material. -Mechanika. -Kaunas: Technologija, 2007, Nr.66(4), p.12-17.

13. **Procopio, A.T., Zavaliangos, A.** Simulation of multiaxial compaction of granular media from loose to high relative densities. -Journal of the Mechanics and Physics of Solids, 2005, 53, p.1523-1551.

14. **Markauskas, D.** Discrete element modelling of complex axisymmetrical particle flow. -Mechanika. -Kaunas: Technologija, 2006, Nr.6(62), p.32-38.

15. **Džiugys, A., Navakas, R.** The role of friction on size segregation of granular material. -Mechanika. -Kaunas: Technologija, 2007, Nr.4(66), p.59-68.

16. **Moreno-Atanasio, R., Anthony, S.J.** Micromechanical behaviour of granular media: effects of contact stiffnesses. In: Topping BHV, Montero GP, Montenegro R, editors. -Proceedings of the Fifth International Conference on Engineering Computational Technology. Stirlingshire: Civil-Comp Press, 2006, p.1-13.

17. **Hentz, S., Donzé, F.V., Daudeville, L.** Discrete element modelling of concrete submitted to dynamic loading at high strain rates. -Computers & Structures, 2004, 82, p.2509-2524.

18. **Antonyuk, S., Khanal, M., Tomas, J., Heinrich, S., Morl, L.** Impact breakage of spherical granules: Experimental study and DEM simulation. -Chemical Engineering and Processing, 2006, 45, p.838-856.

19. **Mishra, B.K., Thornton, C.** Impact breakage of particle agglomerates. -Int. J. Miner. Process, 2001, 61, p.225-239.

20. **D'Addetta, G.A., Ramm, E.** A microstructure-based simulation environment on the basis of an interface enhanced particle model. -Granular Matter, 2006, 8, p.159-174.

21. **Gethin, D.T., Ransing, R.S., Lewis, R.W., Dutko, M., Crook, A.J.L.** Numerical comparison of a deformable discrete element model and equivalent continuum analysis for the compaction of ductile porpous material. -Computers & Structures, 2001, 79, p.1287-1294.

22. **Grest, G.S., Duenweg, B., Kremer, K.** Vectorized link cell fortran code for molecular dynamics simulations for a large number of particles. -Computer Physics Communications, 1989, 55(3), p.269-285.

23. **Balevičius, R., Džiugys, A., Kačianauskas, R.** Discrete element method and its application to the analysis of penetration into granular media. -J. of Civil Engineering and Management, 2004, 10(1), p.3-14.

24. **Balevičius, R., Kačianauskas, R., Džiugys, A., Maknickas, A., Vislavičius, K.** DEMMAT code for numerical simulation of multi-particle dynamics. -Information Technology and Control, 2005, 34(1), p.71-78.

25. **Allen, M.P., Tildesley, D.J.** Computer Simulation of Liquids. -Oxford: Clarendon Press, 1991.-385p.

26. **Maknickas, A., Kačeniauskas, A., Kačianiauskas, R., Belevičius, R., Džiugys, A.** Parallel DEM software for simulation of granular media. -Informatika, 2006, 17(2), p.207-224.

27. **Jiang, M.J., Konrad, J.M., Leroueil, S.** An efficient technique for generating homogeneous specimens for DEM studies. -Computers & Geotechnics, 2003, 30(7), p.579-697.

28. **Heyliger, P.R., McMeeking**, **R.M.** Cold plastic compaction of powders by a network model. -Journal of the Mechanics and Physics of Solids, 2001, 49, p.2031-2054.

29. **Arzt, E.** The influence of an increasing particle coordination on the densification of spherical powders. -Acta Metallurgica et Materialia, 1982, 30, p.1883-90.

30. **Fleck, N.A.** On the cold compaction of powders. -J. of Mechanics and Physics of Solids, 1995, 43, p.1409-31.

31. **Sridhar, I., Fleck, N.A.** Yield behaviour of cold compacted composite powders. -Acta Materialia, 2000, 48, p.3341-3352.

A. Maknickas, R. Kačianauskas, R. Kutas

VIENTISO BANDINIO GENERAVIMAS DISKREČIOMIS DALELĖMIS GNIUŽDYMO TESTUI ATLIKTI

R e z i u m ė

Remiantis fizikinės darnos idėja, nagrinėjamas vientiso bandinio generavimas diskretinių elementų metodu. Bandinio formavimas apima triašio sutankinimo ir laisvo stabilizavimo, įvykus staigiai fragmentacijai, etapus. Sutankinimas apima dujinės fazės virsmą į vientisą kūną. Buvo nagrinėjami mono ir polidispersiniai dalelių rinkiniai. Modeliavimo kokybė buvo vertinama tiriant tankio, slėgio ir koordinačių skaičiaus pokyčius. Bandinio būsenos buvo vertinamos nagrinėjant kinetinę energiją ir formos distorsiją. Gauti skaitiniai rezultatai palyginti su žinomais sprendiniais ir kitų tyrimų duomenimis. Rezultatai parodė,

kad polidispersinė struktūra tiksliau atspindi makroskopinį tamprumo modulį.

A. Macknickas, R. Kačianauskas, R. Kutas

GENERATION OF SOLID SPECIMEN FOR COMPRESSION TESTS BY DISCRETE PARTICLES

S u m m a r y

Physically adjustable concept and discrete element simulations aimed at generating a solid specimen for the compression test is investigated. The suggested scheme comprises triaxial compacting and load-free stabilisation after instantaneous fragmentation. Compacting involves the contact-less gas phase and transition to solid phase. Two compositions of monosized and polydispersed particles are simulated numerically. Simulation quality during compacting is controlled by considering packing density, wall pressure and coordination number. Quality of the final state is evaluated by kinetic energy and shape distortion. Obtained numeric results were compared with other known solutions and data. Results showed that polydispersed structure more correctly represents macroscopic elasticity modulus.

А. Макницкас, Р. Качянаускас, Р. Кутас

ГЕНЕРИРОВАНИЕ СПЛОШНОГО ОБРАЗЦА ДИСКРЕТНЫМИ ЧАСТИЦАМИ ДЛЯ ТЕСТОВ СЖАТИЯ

Р е з ю м е

Исследовано генерирование сплошного образца дискретными частицами. Генерирование охватывало трехосное сжатие и свободную релаксацию после мгновенного сцепления частиц. Уплотнение включает бесконтактную газовую фазу и переход в твердую фазу. Численно изучены два разных образца из моно и полидисперсных частиц. Качество числовых результатов во время уплотнения было подвержено контролю, по плотности упаковки, давлению на стены и числу сцеплений. Качество финального состояния было оценено по кинетической энергии и дисторсии формы. Полученные цифровые результаты сравнены с известными решениями и данными других исследований. Результаты показали, что полидисперсная структура точнее отражает макроскопический модуль упругости.